Biomaterials 32 (2011) 8097–8107

Contents lists available at ScienceDirect

Biomaterials

journal homepage: www.elsevier.com/locate/biomaterials

Bioprinting of growth factors onto aligned sub-micron fibrous scaffolds for simultaneous control of cell differentiation and alignment

Elmer D.F. Ker [a,d], Amrinder S. Nain [e,**], Lee E. Weiss [b,c,d], Ji Wang [e], Joseph Suhan [a], Cristina H. Amon [f], Phil G. Campbell [a,c,d,*]

[a] Department of Biological Sciences, Carnegie Mellon University, Pittsburgh, PA 15213, USA
[b] Robotics Institute, Carnegie Mellon University, Pittsburgh, PA 15213, USA
[c] Institute for Complex Engineered Systems, Carnegie Mellon University, Pittsburgh, PA 15213, USA
[d] McGowan Institute for Regenerative Medicine, UPMC, Pittsburgh, PA 15219, USA
[e] Department of Mechanical Engineering, MC 0238 Randolph Hall, Mechanical Engineering, Virginia Tech, Blacksburg, VA 24061, USA
[f] Department of Industrial and Mechanical Engineering, University of Toronto, Toronto, ON M5S 1A4, Canada

ARTICLE INFO

Article history:
Received 31 May 2011
Accepted 8 July 2011
Available online 5 August 2011

Keywords:
Bone
Muscle
Tendon
Growth factors

ABSTRACT

The capability to spatially control stem cell orientation and differentiation simultaneously using a combination of geometric cues that mimic structural aspects of native extracellular matrix (ECM) and biochemical cues such as ECM-bound growth factors (GFs) is important for understanding the organization and function of musculoskeletal tissues. Herein, oriented sub-micron fibers, which are morphologically similar to musculoskeletal ECM, were spatially patterned with GFs using an inkjet-based bioprinter to create geometric and biochemical cues that direct musculoskeletal cell alignment and differentiation *in vitro* in registration with fiber orientation and printed patterns, respectively. Sub-micron polystyrene fibers (diameter ~ 655 nm) were fabricated using a Spinneret-based Tunable Engineered Parameters (STEP) technique and coated with serum or fibrin. The fibers were subsequently patterned with tendon-promoting fibroblast growth factor-2 (FGF-2) or bone-promoting bone morphogenetic protein-2 (BMP-2) prior to seeding with mouse C2C12 myoblasts or C3H10T1/2 mesenchymal fibroblasts. Unprinted regions of STEP fibers showed myocyte differentiation while printed FGF-2 and BMP-2 patterns promoted tenocyte and osteoblast fates, respectively, and inhibited myocyte differentiation. Additionally, cells aligned along the fiber length. Functionalizing oriented sub-micron fibers with printed GFs provides instructive cues to spatially control cell fate and alignment to mimic native tissue organization and may have applications in regenerative medicine.

1. Introduction

Musculoskeletal tissues comprise multiple cell types such as osteoblasts, tenocytes and myocytes arrayed within a spatially-graded structural and biochemical microenvironment. The native organization of these tissues is regulated, in part, by microenvironmental instructive signals such as growth factor (GF) biochemical cues and ECM architectural geometric cues to modulate stem cell behaviors such as differentiation and cell alignment during repair and regeneration [1–5].

Within the pericellular microenvironment, signaling molecules such as GFs, can exist in both 'liquid-phase' (freely diffusing in solution) and 'solid-phase' (immobilized and bound to the ECM and cell surfaces) forms [4]. When bound to the ECM, GFs are immobilized at picograms to nanogram quantities and impart temporal and spatial cues that regulate cell behaviors such as cell adhesion, migration, proliferation, differentiation and apoptosis [4–12].

In muscle, tendon and bone tissues, differentiated cell types such as myocytes, tenocytes and osteoblasts maintain tissue function by contractile force generation, collagen secretion and collagen mineralization, respectively. In addition, cell orientation plays an integral role since myocyte alignment is necessary for efficient force generation along a specific direction during muscle contraction [13–15], while tenocyte and osteoblast alignment are required for building highly oriented unmineralized and mineralized collagen matrices that can withstand mechanical loading during

* Corresponding author. 1201 Hamburg Hall, 5000 Forbes Ave, Carnegie Mellon University, Pittsburgh, PA 15213, USA. Tel.: +1 412 268 4126; fax: +1 412 268 5229.
** Corresponding author.
E-mail addresses: nain@vt.edu (A.S. Nain), pcampbel@cs.cmu.edu (P.G. Campbell).

0142-9612/$ – see front matter © 2011 Published by Elsevier Ltd.
doi:10.1016/j.biomaterials.2011.07.025

skeletal movement [1,16–20]. Furthermore, it has recently been shown that aligned fibrous scaffolds promoted increased calcium content and mineralization in comparison with unaligned fibrous scaffolds in a manner independent of increased cell proliferation or increased mRNA expression of osteogenic markers [18].

Although there have been numerous investigations using exogenous biochemical cues to control musculoskeletal stem cell differentiation [21–26], and engineered geometric cues to control cell alignment [14,27–29], such work has yet to address simultaneous control of both cell alignment and differentiation at high spatial resolution.

We previously developed an inkjet-based bioprinter [6] that spatially patterns low doses (picograms to nanograms) of GFs and other signaling molecules onto and into native ECM-based scaffolds, including fibrin and acellular human skin allografts. The printed GFs subsequently bind to the ECM via native binding affinities to create physiologically-relevant solid-phase GF patterns that can control aspects of stem cell behavior such as differentiation, migration and proliferation *in vitro* [6,8–12] and *in vivo* [7] in spatial registration with printed patterns. One advantage of using such an approach is that it can provide persistent biochemical cues for directing a single stem cell population towards multiple cell fates such as muscle, tendon and bone cells simultaneously within a single construct [8,12]. In addition, we have also developed a novel pseudo-dry spinning technique that creates highly oriented sub-micron fibers as a means to control cell alignment [30,31]. In the present study, bioprinted GFs were patterned onto fibrin- or serum-coated highly oriented sub-micron polystyrene fibers fabricated with our Spinneret-based Tunable Engineered Parameters (STEP) technique [30,31] to study the interactions of biochemical and geometrical cues on stem cell differentiation and alignment. This study was performed in the context of using the aligned fiber scaffolds patterned with GFs to spatially control stem cell differentiation towards myocyte, tenocyte and osteoblast fates simultaneously *in vitro* while also controlling cell alignment to create a primitive muscle-tendon-bone unit.

2. Materials and methods

2.1. Fabrication of polystyrene STEP fibers

To facilitate comparison of cell alignment between STEP fibers and standard tissue culture vessels, polystyrene STEP fibers were used. In addition, polystyrene is non-resorbable and removes the resorption variable from this study. Sub-micron, oriented polystyrene STEP fibers were fabricated using the STEP pseudo-dry spinning process as previously described [30,31] (Fig. 1). Briefly, a glass micropipette was mounted on a manual XYZ stage (562 Ultra-align series, Newport Inc., USA) and oriented perpendicularly to a rotating cover slip substrate mounted on a DC motor. The DC motor was mounted on a motorized XYZ nanopositioner (Newport VP series, Irvine, CA). Polystyrene (2×10^6 g/mol, Scientific Polymer Products, USA, dissolved in Xylene 10% by weight) was drawn out and extruded through the pipette and continuously wound around the rotating substrate, becoming fibers as the solvent evaporated. By controlling the speeds of the nanopositioner and rotating motor, scaffolds with defined sub-micron fiber diameters and fiber spacing were fabricated. In addition, subsequent layers can be deposited on top of existing fiber layers and at other orientations to produce, for example, criss-cross fiber patterns that were oriented perpendicular to one another. In addition, aligned fibers wound around a hollowed-out substrate support base can be fabricated to form suspended fibrous structures.

2.2. Coating fibrin or serum on of polystyrene STEP fibers

Polystyrene STEP fibers were sterilized with 70% ethanol for 5 min, rinsed with Phosphate Buffered Saline (PBS), and subsequently coated with serum by incubation in 100% serum overnight at room temperature (RT). Excess unbound serum proteins were removed by aspiration, rinsed with PBS and air-dried in a laminar flow hood.

For fibrin coating, polystyrene STEP fibers were first coated with fibrinogen by incubation in 0.1 mg/mL fibrinogen (Aventis Behring, King of Prussia, PA or American Diagnostica Inc., Stamford, CT) contained in 10 mM sodium phosphate, pH 7.4 overnight at RT. Excess unbound fibrinogen was removed by aspiration, rinsed with PBS and fibers were blocked with 0.3 M glycine (Bio-Rad Laboratories, Hercules, CA), pH 7.4 for 2 h at RT. Immobilized fibrinogen was converted into fibrin by incubating fibers in 4 U/mL thrombin (Enzyme Research Laboratories, South Bend, IN) for 2 h at 37 °C, rinsed three times with PBS followed by three rinses with sterile deionized water before air-drying in a laminar flow hood. To confirm that the polystyrene STEP fibers were successfully coated with fibrin, Alexa Fluor 647-conjugated fibrinogen (Invitrogen, Carlsbad, CA) was used.

2.3. Scanning electron microscopy

To characterize the diameter of the polystyrene STEP fibers, samples were gold-coated using a Pelco SC-6 sputter coater (Ted Pella, Inc., Redding, CA) and examined using a Hitachi 2460N Scanning Electron Microscope (Hitachi High Technologies America, Inc., Schaumburg, IL). Images were obtained using Quartz PCI Image software.

For cell-seeded STEP fibers, cells were washed once in PBS and subsequently fixed using 2.5% glutaraldehyde in PBS and prepared for SEM. After three PBS washes, the specimens were fixed for 1 h in 1% osmium tetroxide buffered with PBS. The osmium tetroxide was removed with three washes of DI water for 5 min followed by incubation for 5 min in 1% thiocarbohydrazide in DI water. The specimens were washed three times in DI water followed by a 5 min exposure to 1% osmium tetroxide in DI water. The specimens were washed with three changes of DI water, and after the exposure to thiocarbohydrazide, the DI water washes, and treatment with osmium tetroxide was repeated. After fixation, the specimens were washed with three changes of DI water followed by dehydration in an ascending series of ethanol (50%, 70%, 80%, 90%, and 3 changes of 100%). The specimens were dried in a Pelco CPD2 critical point dryer (Ted Pella, Inc., Redding, CA) using carbon dioxide at 1200 psi, and 42 °C. Dried specimens were attached to SEM stubs using double-sided stick tape and coated with gold using a Pelco SC-6 sputter coater (Ted Pella, Inc., Redding, CA). Specimens were examined using a Hitachi 2460N Scanning Electron Microscope (Hitachi High Technologies America, Inc., Schaumburg, IL). Images were obtained using Quartz PCI Image software.

2.4. Transmission electron microscopy

To characterize polystyrene STEP fibers, samples were placed in a 35 mm Petri-dish and coated with gold using a Pelco SC-6 sputter coater (Ted Pella, Inc., Redding, CA). Subsequently, the Petri dishes were filled with Epon-Araldite and were infiltrated for at least three days at room temperature and placed in an oven at 30 °C for 24 h, at 40 °C for 24 h, at 50 °C for 24 h and finally at 60 °C overnight to allow for slow polymerization of the Epon-Araldite. The samples were cut to fit into an embedding capsule and re-embedded in Epon-Araldite. Thin (100 nm) cross sections of the re-embedded sample were cut using a Reichert-Jung Ultracut E and a DDK Diamond knife. When required, the sections were stained with 1% uranyl acetate and Reynold's lead citrate before viewing on a Hitachi 7100 transmission electron microscope. Digital images were obtained using an AMT Advantage 10 CCD Camera System and NIH Image software.

2.5. Cell culture

Multipotent C3H10T1/2 cells (ATTC, Manassas, VA) were grown in Dulbecco's Modified Eagle's Media (DMEM; Invitrogen, Carlsbad, CA), 10% fetal bovine serum (Invitrogen, Carlsbad, CA) and 1% penicillin-streptomycin (PS; Invitrogen, Carlsbad, CA). C2C12 cells (ATTC, Manassas, VA) were grown in DMEM, 10% bovine serum (Invitrogen, Carlsbad, CA) and 1% PS. Cells were seeded onto polystyrene STEP fibers in a 50–70 μL droplet containing ~ $10–15 \times 10^4$ cells and allowed to attach for 1.5 h before flooding the dish with complete media. In experiments utilizing fibrin-coated fibers, a final concentration of 1 μg/mL aprotinin was added to complete media to minimize fibrin degradation (Sigma Aldrich, St. Louis, MO). All cells were kept at 37 °C, 5% CO_2 in a humidified incubator.

2.6. Growth factor bioprinting

Prior to printing, GFs were freshly diluted to the desired concentration in 10 mM sodium phosphate, pH 7.4. Prior to filling the inkjet with a GF, the printhead was sterilized by rinsing with 70% ethanol followed by sterile deionized water. The bio-ink, consisting of 50–100 μg/ml GF was loaded into the printhead, and printed as previously described [6,11]. The deposited concentration of inkjetted GFs was modulated by overprinting, which is achieved by varying the number of times a GF is deposited in the same (x,y) location. After printing, fibrin-coated STEP fibers were incubated in serum-free DMEM with 1% PS overnight at 37 °C, 5% CO_2 to wash off unbound GF prior to cell seeding. The surface concentration of GF present on fibrin-coated STEP fibers prior to cell seeding was estimated based on the desorption measurements from previous studies [6,9,11,32].

2.7. Alkaline phosphatase (ALP) staining

Staining for the osteoblast marker Alkaline Phosphatase (ALP) was performed using an ALP staining kit (Kit 86C, Sigma Aldrich, St. Louis, MO) according to the manufacturer's instructions.

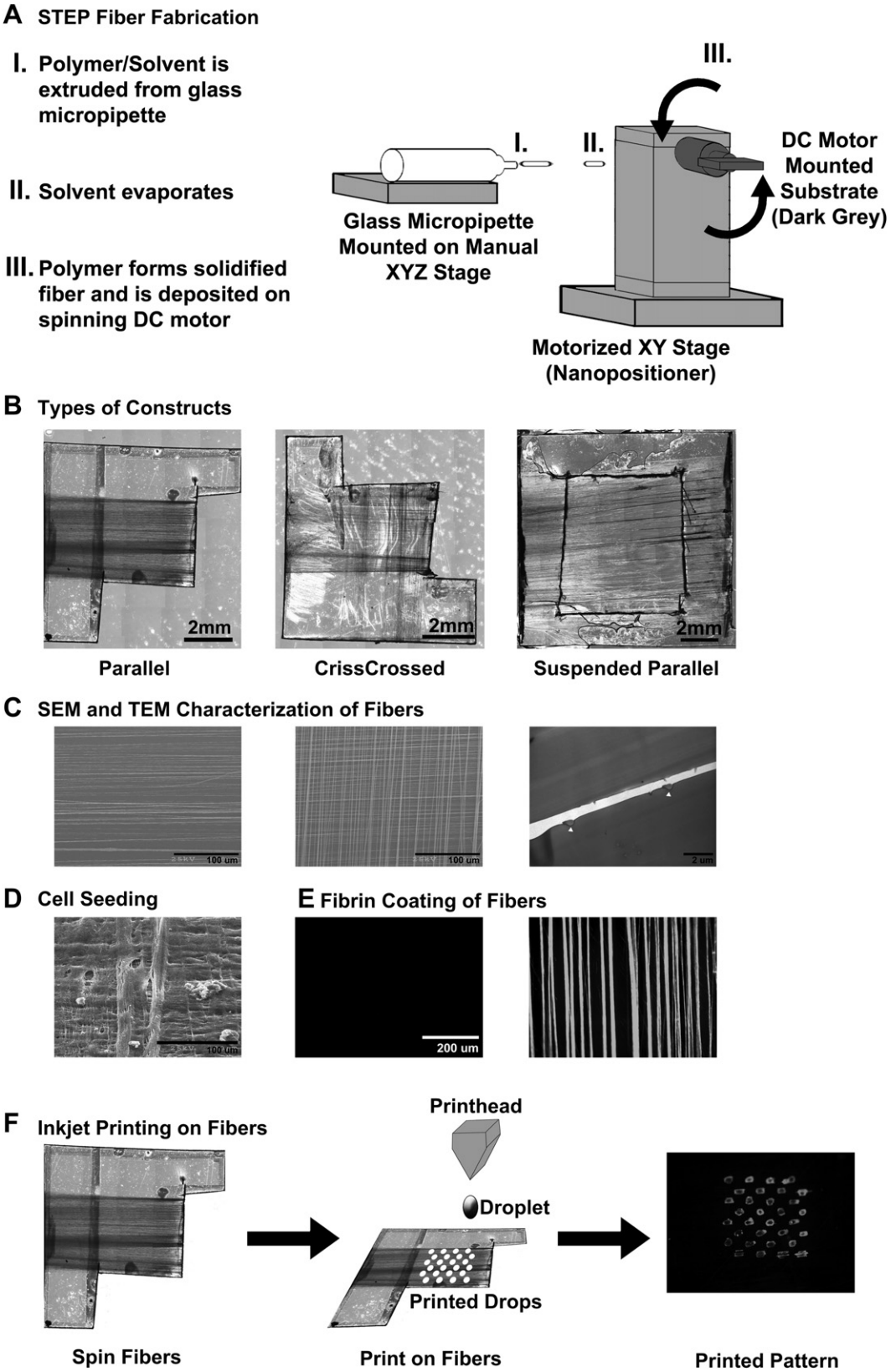

Fig. 1. Polystyrene Spinneret-based Tunable Engineered Parameter (STEP) sub-micron fibers. A. Scheme illustrating STEP fiber fabrication. B. Types of STEP fibers that can be fabricated. The left scaffold consists of one set of fibers running in a parallel manner. The middle scaffold consists of two sets of fibers running perpendicular to each other. The right scaffold consists of one set of fibers running in a parallel manner with a hollowed-out support base. C. Typical SEM and TEM images of STEP fibers used for quantifying diameter length. D. Typical SEM image showing attachment of cells to polystyrene STEP fibers. E. Coating of polystyrene STEP fibers with Alexa649-conjugated fibrin. Left image shows uncoated STEP fibers while right image shows fibrin-coated STEP fibers. Some fibers aggregate to form larger fiber bundles after numerous washing steps. F. Inkjet printing indicates that polystyrene STEP fibers can be printed on. Scale bars are as indicated.

Table 1
Characterization of polystyrene STEP fibers.

	Data ± Standard Error Mean
Scanning Electron Microscopy (n = 43)	668 ± 34 nm
Transmission Electron Microscopy (n = 20)	628 ± 63 nm
Linearity of Fibers with respect to one another (n = 45)	2.54 ± 0.24 degrees

2.8. Immunofluorescence staining

Cells were washed in PBS, fixed in methanol for 5 min, air-dried and blocked with 10% donkey serum (Jackson Immunoresearch, West Gove, PA) for 20 min at RT. For mouse-on-mouse staining, an additional blocking step was performed by incubating cells with 100 μg/mL donkey anti-mouse FAB (Jackson Immunoresearch, West Gove, PA) for 1 h at RT. Cells were then rinsed with wash buffer (PBS, 0.1% BSA) and incubated with primary antibodies: rabbit anti-scx (10 μg/mL; Abcam, Cambridge, MA) and/or mouse anti-myosin MF20 (1 μg/mL; Developmental Studies Hybridoma Bank, Iowa City, Iowa) overnight at 4 °C. Cells were then rinsed three times with wash buffer (5 min each) and incubated with secondary antibodies for 1 h at RT—donkey anti-mouse Dylight 488 nm or donkey anti-rabbit Dylight 549 nm (15 μg/mL each; Jackson Immunoresearch, West Gove, PA). Lastly, cells were rinsed five times with wash buffer (5 min each) and imaged using a Zeiss Axiovert 200M microscope (Carl Zeiss Microimaging, Thornwood, NY) equipped with a Colibri LED light source.

2.9. Quantification of immunofluorescence or ALP staining

When required, suspended parallel STEP fibers were subsequently transferred to a fresh dish after staining to rule out the possibility that cells below the fibrous layer (either on the support substrate or dish bottom) were aligning or responding to the printed GF patterns. This procedure ensured that any positive signals observed originated only from cells that had attached to the fibers. Quantification of immunofluorescence or ALP staining was performed using Adobe Photoshop 7.0 (Adobe Systems, San Jose, CA). Briefly, the rectangular marquee tool was used to draw a bounding box (depending on the size of the printed pattern and/or magnification) and the image histogram tool was used to measure average pixel intensity. As an alternative to using average pixel intensity, the number of myotubes greater than 250 μm in length was manually counted. Error bars were expressed as standard error of the mean (SEM).

2.10. Actin staining

To determine the cytoskeletal arrangement of cells within GF-printed regions of STEP fibers, fibrin-coated STEP fibers were soaked or hand-printed with BMP-2 or FGF-2. The soaking mimicked the action of GF printing and facilitated these studies because the precise determination of GF-printed boundaries was not required. Briefly, a 50–70 μL of a 100 μg/mL GF solution was pipetted onto fibrin-coated STEP fibers (enough to cover the entire scaffold) and the GF was allowed to air-dry at 37 °C. After drying, GF-soaked STEP fibers were stored at 4 °C prior to cell seeding. 24 h post cell seeding, the GF-soaked fibrin-coated STEP fibers were washed twice in PBS and fixed in methanol-free 4% paraformaldehyde for 10 min. The fixative was aspirated and cells were washed twice in PBS and permeabilized with 0.1% Triton X-100 (Sigma Aldrich, St. Louis, MO) for 5 min. Cells were washed twice in PBS and blocked with wash buffer (PBS, 0.1% BSA) for 20 min at RT to reduce non-specific staining. Cells were subsequently washed twice in PBS before adding Alexa Fluor 647-conjugated phalloidin (Invitrogen, Carlsbad, CA) according to the manufacturer's instructions (5 μL stock solution for every 200 μL PBS). Lastly, cells were washed twice in PBS and imaged using a Zeiss LSM 510 Meta NLO Confocor 3 inverted spectral confocal microscope (Carl Zeiss Microimaging, Thornwood, NY).

2.11. Statisical analysis

Quantification of immunofluorescence measurements were analyzed using one-way analysis of variance followed by Fisher's least significant difference post hoc test using SYSTAT 9 software (Systat Software Inc., Richmound, CA) to determine significance among treatment groups. A p value ≤ 0.05 was considered statistically significant.

3. Results

3.1. Characterization of polystyrene STEP fibers

Fig. 1 illustrates the fabrication and characteristics of polystyrene STEP fibers. Briefly, during the process of pseudo-dry spinning, the solvent is evaporated by the surrounding ambient air as it is

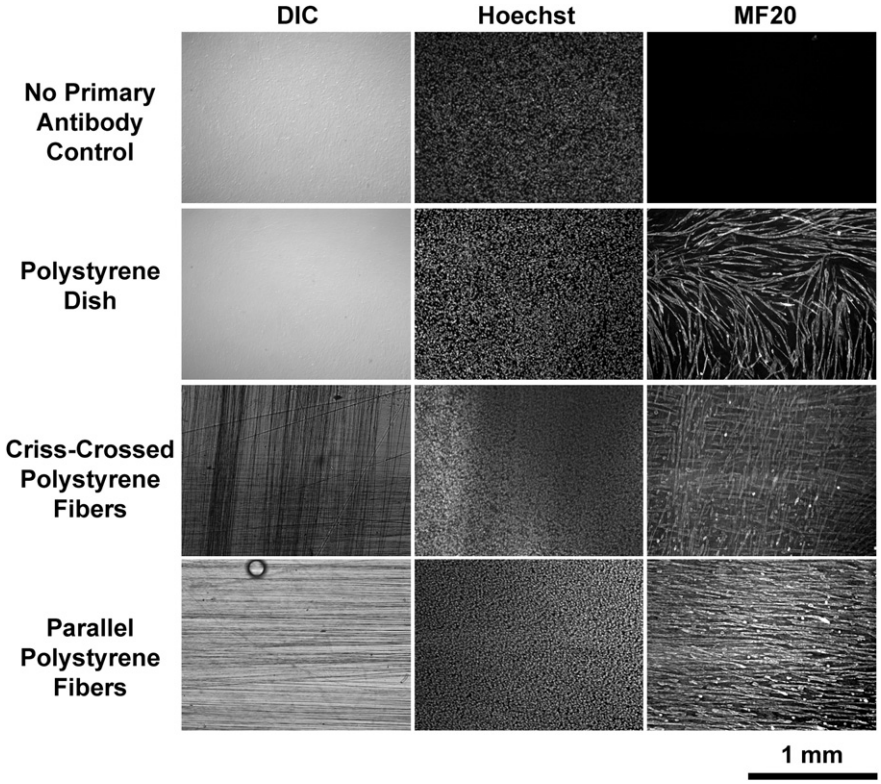

Fig. 2. Effect of polystyrene STEP fiber organization on myotube alignment. Under conditions of high cell density, C2C12 cells spontaneously form elongated myotubes that are randomly oriented in a polystyrene dish. On criss-crossed and parallel polystyrene STEP fibers, C2C12 cells form elongated myotubes that align along the fiber length. No MF20 signal is observed in the no primary antibody control. Scale bar 1 mm.

extruded from the micropipette (Fig. 1A). This increases the local concentration of polystyrene and promotes entanglement of polystyrene chains, which reduces chain mobility and starts the process of forming a solidified fiber [30,31]. By choosing an appropriate DC motor speed to control fiber deposition as well as controlling the vertical speed of the nanopositioner to affect fiber spacing, scaffolds with parallel fibers are fabricated (Fig. 1B, left panel). Furthermore, multiple layers can be deposited to produce criss-crossed fibers (Fig. 1B, middle panel). In addition, these fibers can be spun on a hollowed-out support base to produce suspended fibers (Fig. 1B, right panel). SEM and TEM analysis of the fibers indicate that polystyrene STEP sub-micron fibers had a diameter of 668 ± 34 nm and 628 ± 63 nm, respectively (Table 1, Fig. 1C). Fibers were predominantly oriented in parallel arrays and deviated less than 2.54 ± 0.24 degrees with respect to one another (Table 1). SEM analysis also showed that polystyrene STEP fibers allowed for cell attachment and promoted cell alignment (Fig. 1D). Lastly, polystyrene STEP fibers could be coated with various ECM proteins such as fibrin and printed on (Fig. 1E,F). Fibrin-coating of polystyrene STEP fibers was also confirmed by TEM analysis (Supplementary Figure 1).

3.2. Effect of polystyrene STEP fibers on myotube alignment

Having characterized the structural properties of the polystyrene STEP fibers, Fig. 2 shows the geometric effect of polystyrene STEP fiber organization on C2C12 cells. Under conditions of high cell density, C2C12 cells spontaneously form elongated myotubes that are randomly oriented in a polystyrene dish. However, when seeded onto criss-crossed and parallel polystyrene STEP fibers, C2C12 cells form elongated myotubes that aligned along the fiber length (Fig. 2).

3.3. Effect of serum-coated STEP fibers patterned with FGF-2 on tenocyte differentiation

Given that polystyrene STEP fibers control cell alignment, these scaffolds were coated with serum and subsequently printed with FGF-2 patterns to determine if these patterns could drive C3H10T1/2 cell differentiation towards a tenocyte fate. As can be seen in Fig. 3, our bio-inkjet printing technology allows for controlled deposition of varying amounts of GFs such as FGF-2 in a spatially

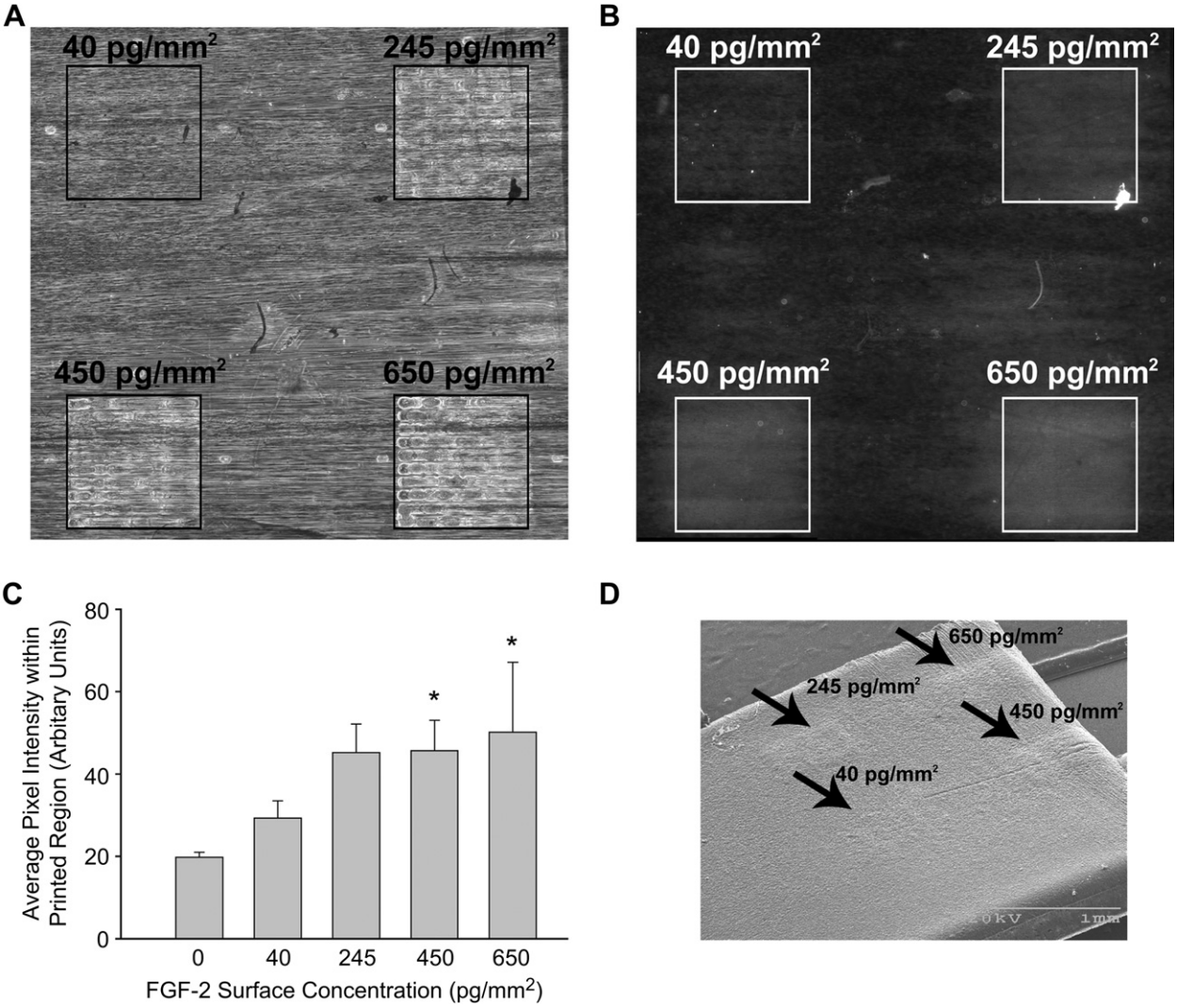

Fig. 3. Effect of Printed FGF-2 patterns on Scx expression in C3H10T1/2 cells. A. Phase-contrast image showing serum-coated STEP fibers post-FGF-2 printing. 2, 12, 22 and 32 Overprints of 100 μg/mL FGF-2 corresponding to 40 pg/mm², 245 pg/mm², 450 pg/mm² and 650 pg/mm² FGF-2 were printed. Black boxes indicate 1 × 1 mm printed regions. B. On serum-coated STEP fibers, C3H10T1/2 cells show a dose-dependent increase in Scx (tenocyte) staining with increased FGF-2 overprints. White boxes indicate 1 × 1 mm printed regions. C. Quantification of Scx signal within printed regions ($n = 3$). Error bars indicate ± SEM. *, Significantly different from non-printed control regions; $p \leq 0.05$. D. SEM image showing serum-coated STEP fibers post-cell seeding. Black arrows and corresponding text indicate printed regions. Scale bar 1 mm.

precise manner (Fig. 3A), which results in a dose-dependent increase in expression of the tendon marker Scleraxis (Scx) in C3H10T1/2 cells (Fig. 3B,C). Although lower doses of FGF-2 (40 pg/mm^2 and 245 pg/mm^2 FGF-2) immobilized to the scaffold (referred to as 'solid-phase' FGF-2) were not sufficient to induce an increase in the expression of the tenocyte marker Scx relative to non-printed control regions ($p = 0.428$ for 40 pg/mm^2 FGF-2 and $p = 0.052$ for 245 pg/mm^2 FGF-2), higher doses of solid-phase FGF-2 (450 pg/mm^2 and 650 pg/mm^2 FGF-2) resulted in an increase in Scx expression relative to non-printed control regions ($p = 0.048$ for 450 pg/mm^2 FGF-2 and $p = 0.025$ for 650 pg/mm^2 FGF-2; Fig. 3) in C3H10T1/2 cells. SEM analysis verified that printed FGF-2 remain bound to serum-coated polystyrene STEP fibers as evidenced by the square bumps which indicate increased cell proliferation on mitogenic FGF-2 patterns (Fig. 3D).

3.4. Effect of fibrin-coated STEP fibers patterned with BMP-2 on osteoblast differentiation

Having demonstrated that printed FGF-2 patterns could induce stem/progenitor cells towards a tendon lineage, polystyrene STEP fibers were coated with fibrin and printed with BMP-2 to determine if osteoblast differentiation could be patterned. As can be seen in Fig. 4, printed patterns of BMP-2 show increased expression of the osteoblast marker, alkaline phosphatase (ALP) relative to non-printed control regions ($p \leq 0.001$) in C2C12 cells (Fig. 4).

3.5. Effect of fibrin-coated STEP fibers patterned with FGF-2 on tenocyte and myocyte differentiation and cell alignment

To determine if cell alignment and cell differentiation could be controlled simultaneously on oriented fibers printed with a single GF, patterns of FGF-2 were printed onto fibrin-coated STEP fibers and seeded with C2C12 cells. As can be seen in Fig. 5, printed FGF-2 patterns resulted in increased expression of Scx and decreased expression of the muscle marker MF20 in C2C12 cells (Fig. 5). Although a low dose of solid-phase FGF-2 (240 pg/mm^2 FGF-2) was not sufficient to induce an increase in Scx expression relative to 120 pg/mm^2 FGF-2 ($p = 0.494$), higher doses of solid-phase FGF-2 (490 pg/mm^2 and 730 pg/mm^2 FGF-2) resulted in an increase in Scx expression relative to 120 pg/mm^2 FGF-2 ($p = 0.04$ for 490 pg/mm^2 FGF-2 and $p = 0.007$ for 730 pg/mm^2 FGF-2) in C2C12 cells. In

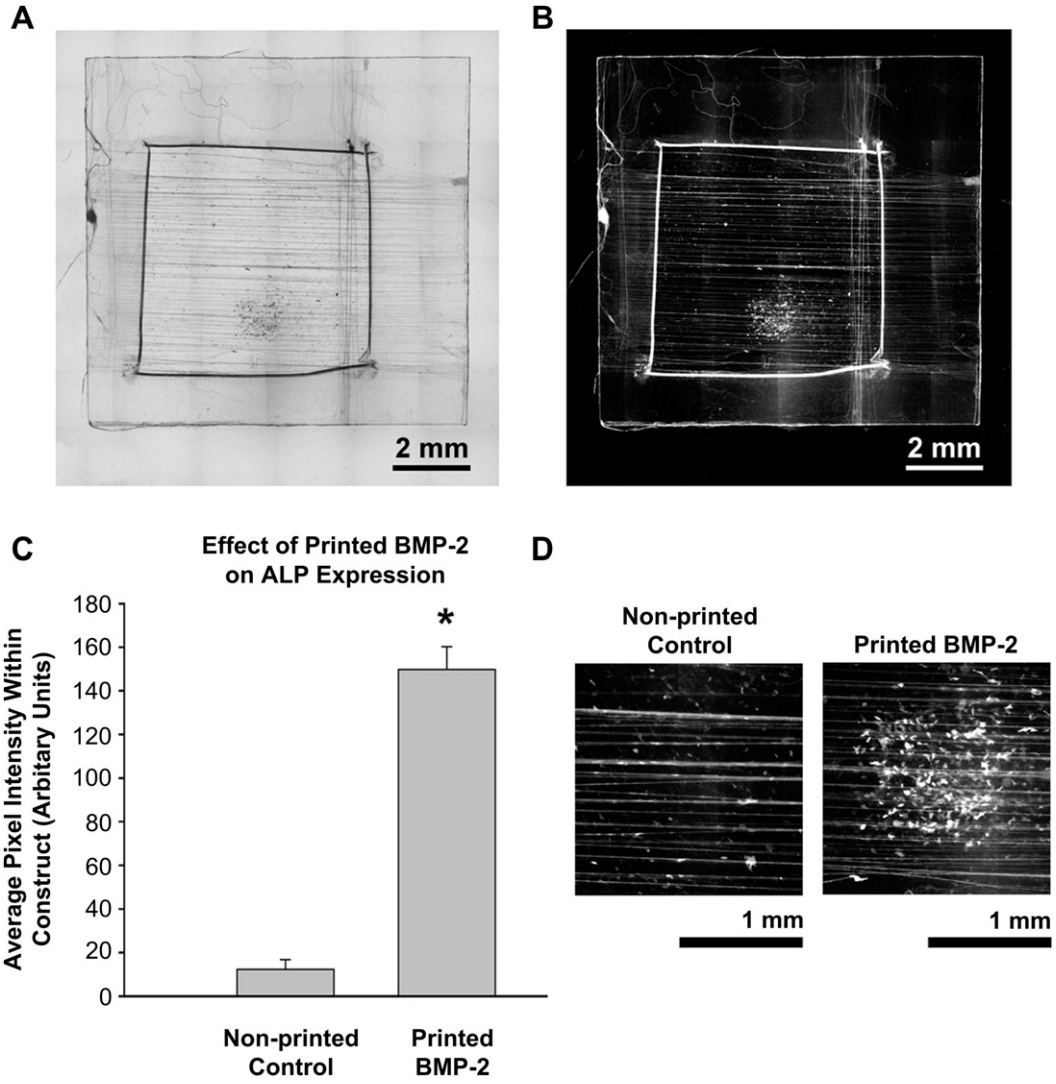

Fig. 4. Effect of printed BMP-2 patterns on ALP expression in C2C12 cells. A. Grey-scaled image of ALP staining. 36 Overprints of 200 μg/mL BMP-2 corresponding to 4 ng/mm^2 BMP-2 were printed onto fibrin-coated STEP fibers. Scale bar 2 mm. B-D. Quantification of ALP staining within printed regions ($n = 5$). Error bars indicate ± SEM. *, Significantly different from control or non-printed regions; $p \leq 0.001$. Scale bars as indicated.

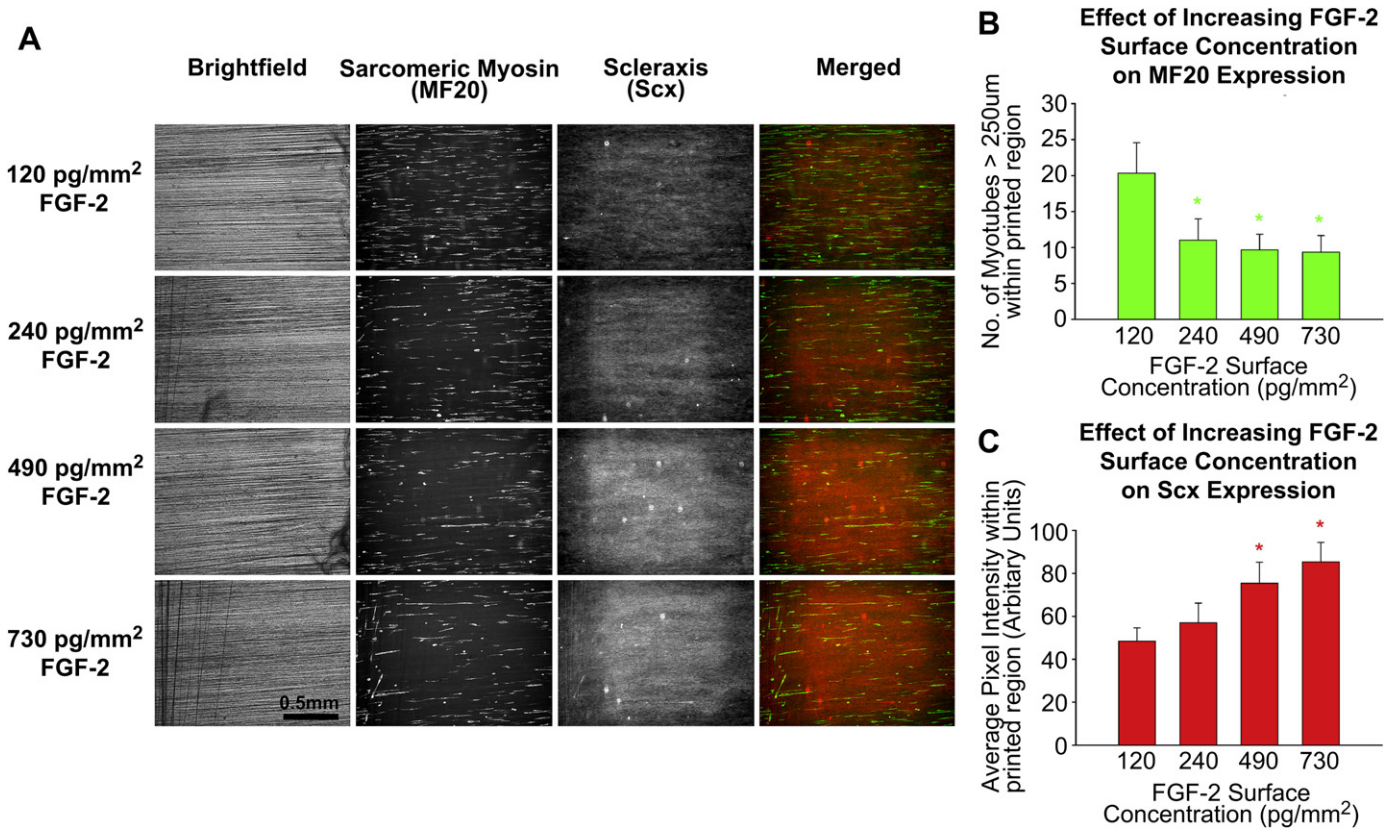

Fig. 5. Effect of printed FGF-2 patterns on MF20 and Scx expression in C2C12 cells. A. 6, 12, 24 and 36 Overprints of 100 μg/mL FGF-2 corresponding to 120 pg/mm^2, 240 pg/mm^2, 490 pg/mm^2 and 730 pg/mm^2 FGF-2 were printed. On fibrin-coated STEP fibers, C2C12 cells show a dose-dependent decrease in MF20 staining and a dose-dependent increase in Scx staining with increasing FGF-2 overprints. Note alignment of myotubes along fiber axis. Scale bar 0.5 mm. B. Quantification of MF20 signal within printed FGF-2 regions ($n = 6$). Error bars indicate ± SEM. *, Significantly different from 6 Overprints (120 pg/mm^2 FGF-2); $p \leq 0.05$. C. Quantification of Scx signal within printed FGF-2 regions ($n = 6$). Error bars indicate ± SEM. *, Significantly different from 6 Overprints (120 pg/mm^2 FGF-2).

addition, increasing doses of solid-phase FGF-2 (240 pg/mm^2, 490 pg/mm^2 and 730 pg/mm^2 FGF-2) inhibited myotube formation relative to 120 pg/mm^2 FGF-2 ($p = 0.043$ for 240 pg/mm^2 FGF-2, $p = 0.022$ for 490 pg/mm^2 FGF-2 and $p = 0.019$ for 730 pg/mm^2 FGF-2). Outside of the printed pattern, cells maintained elongated myotube structures that were aligned in a parallel fashion along the fiber length (Fig. 5A).

3.6. *Effect of fibrin-coated STEP fibers patterned with BMP-2 and FGF-2 on osteoblast, tenocyte and myocyte differentiation and cell alignment*

To determine if cell alignment and multiple differentiation fates could be controlled simultaneously on the same scaffold, patterns of FGF-2 and BMP-2 were printed onto fibrin-coated STEP fibers and seeded with C2C12 cells (Fig. 6A). In this experiment, a suspended scaffold comprised of parallel STEP fibers spun over a hollowed-out base was used for cell seeding (Fig. 1B). This scaffold was subsequently transferred to a fresh dish post-staining to rule out the possibility that cells below the fibrous layer (i.e. cells that had attached onto the support base or dish bottom) were responding to the GF patterns. As can be seen in Fig. 6, printed BMP-2 and FGF-2 patterns resulted in increased expression of the osteoblast marker ALP and tenocyte marker Scx, respectively, while inhibiting myogenesis in C2C12 cells (Fig. 6B,C,D). Expression of ALP within the BMP-2 pattern increased relative to both the printed FGF-2 pattern ($p \leq 0.001$) and non-printed control region ($p \leq 0.001$). Expression of Scx within the FGF-2 pattern was increased relative to non-printed control region ($p = 0.033$) but not to the printed BMP-2 pattern ($p = 0.367$). Concurrently, expression of the muscle marker MF20 was decreased on both printed BMP-2 ($p = 0.015$) and FGF-2 ($p = 0.032$) patterns. Outside of the printed patterns, cells stained positive for the myotube marker MF20 and aligned in a parallel fashion along the fiber length (Fig. 6B,E). To determine the alignment of cells within the printed GF patterns, manual annotation of printed BMP-2 and FGF-2 patterns was performed (Supplementary Figure 2). C2C12 cells adopted a predominantly parallel orientation with respect to the fiber length within and outside of printed regions, indicative of geometric control of cell alignment (Supplementary Fig. 2). To determine the cytoskeletal arrangement of cells within GF-printed regions of STEP fibers, actin staining was performed on C2C12 cells seeded onto fibrin-coated STEP fibers that had been previously pre-soaked in BMP-2 or FGF-2 (Fig. 7). The pre-soaking step mimicked the action of GF printing and facilitated these studies because the precise determination of GF-printed boundaries was not required. Actin staining demonstrated that actin filaments adopted parallel bundles with respect to fiber orientation (Fig. 7, Supplementary Movie 1 and 2).

Supplementary video related to this article can be found at doi:10.1016/j.biomaterials.2011.07.025.

4. Discussion

Our long-term goal is to engineer biomimetic scaffolds for aiding repair of musculoskeletal tissues. In this report, polystyrene sub-micron fibers, approximately 655 nm in diameter, were

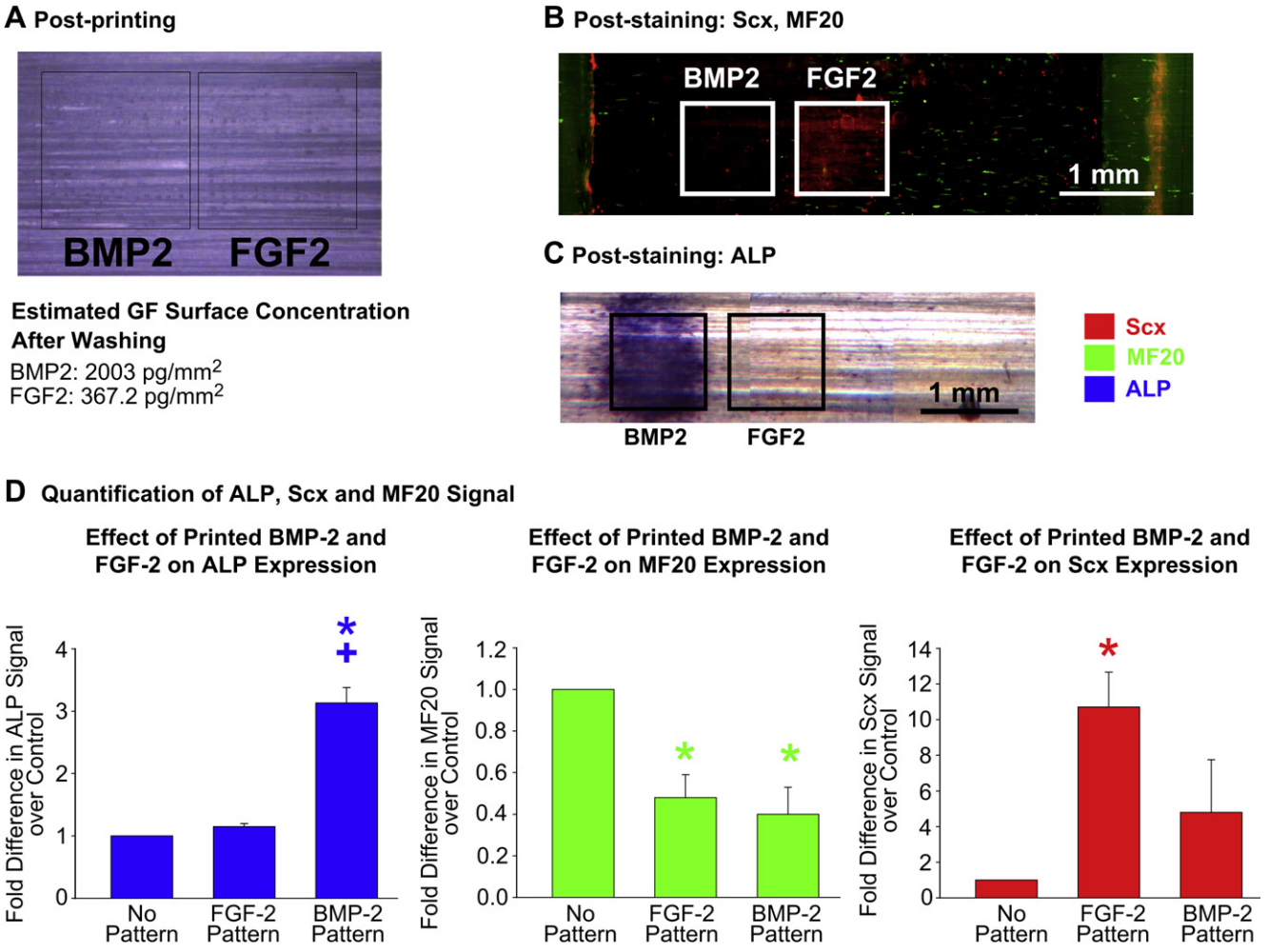

Fig. 6. Effect of printed BMP-2 and FGF-2 patterns on ALP, MF20 and Scx expression in C2C12 cells. A. Post-printing of 100 μg/mL BMP-2 and 50 μg/mL FGF-2 patterns (36 Overprints each) on fibrin-coated STEP fibers. Dark circular shapes within the printed regions (Black boxes) indicate deposited GF droplets. B. On fibrin-coated STEP fibers, C2C12 cells show increased Scx staining on FGF-2 patterns but little to none on BMP-2 patterns. Off-pattern, C2C12 cells form myocytes that are aligned along fiber axis. Scale bar 1 mm. C. On fibrin-coated STEP fibers, C2C12 cells show increased ALP staining on BMP-2 patterns but little to none on FGF-2 patterns. Scale bar 1 mm. D. Quantification of ALP, Scx and MF20 Signal ($n = 4$). Error bars indicate ± SEM. *, Significantly different from control or non-printed regions; $p \leq 0.05$. +, Significantly different from FGF-2-printed regions; $p \leq 0.05$.

fabricated using the STEP technique [30,31], and then coated with ECM material such as serum or fibrin to make the fibers compatible with GF bioprinting (Fig. 1, Supplementary Figure 1). In addition, non-printed and uncoated polystyrene STEP fibers were found to promote myocyte alignment (Fig. 2). This study utilized our established non-biodegradable polystyrene-based STEP fibers [30,31] as a surrogate substrate material suitable for *in vitro* studies. However, for follow-on *in vivo* studies we are developing completely biodegradable STEP fibers made with fibrinogen, poly(lactic-co-glycolic acid)-fibrinogen blends [30,31] or polyurethane (Data not shown). Furthermore, we recently demonstrated that polyurethane STEP fibers can be fibrin-coated,

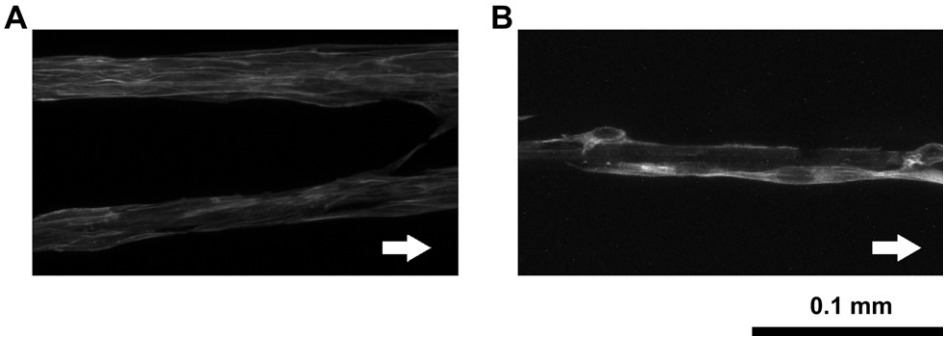

Fig. 7. Effect of fibrin-coated STEP fibers pre-soaked with BMP-2 and FGF-2 on C2C12 cell alignment. A. BMP-2 soaked fibrin-coated STEP fibers. B. FGF-2 soaked fibrin-coated STEP fibers. White arrow indicates fiber orientation. Scale bar 100 μm.

patterned with BMP-2 and induce C2C12 cells towards an osteoblast fate (Data not shown).

Polystyrene-based fibers were fabricated such that the fiber diameter would approximate the diameter of ECM fibers [30,31] and were employed here as an appropriate control since the material used for tissue culture vessels is based on polystyrene. STEP fiber fabrication is based on a recently discovered pseudo-dry spinning technique, which involves extruding a dissolved polymer solution from a glass micropipette spinneret [30,31]. Upon extrusion, the polymer solvent is evaporated by ambient air and the solidified fiber is subsequently deposited on the substrate [30,31]. Similar to electrospinning technique, the STEP technique relies on varying material parameters such as polymer molecular weight and solution polymer concentration to control fiber diameter; however, the fiber distribution and alignment is precisely controlled with the STEP technique by varying the angular and vertical speeds of the rotating substrate [30,31]. Compared to other fiber fabrication platforms, the STEP technique uniquely allows for fabrication of uniform polymer fibers with diameters ranging from sub-50 nm to submicrometer to several millimeters, with highly defined orientations [30,31].

Although the precise mechanism behind geometry-induced cell alignment is presently unknown, it is likely that the alignment of cells observed on fibers may be attributed to a combination of factors including physical space constraint and relative stiffness of the underlying substrate (fiber), ultimately affecting changes in both cell spreading and cell stiffness [14,33–37]. Since cell spreading and cell stiffness are not mutually exclusive phenomena and have been reported to interact in a complex fashion to alter cell morphology [36], cells may be predisposed towards a specific orientation through the modulation of mechanotransduction pathways via cytoskeletal rearrangements. This is evident by the parallel arrangement of actin filaments observed in C2C12 cells grown on GF-soaked fibers (Fig. 7, Supplementary Movie 1 and 2). In the case of higher-ordered structures such as myotubes, which arise from cell-to cell fusion, this predisposition would promote increased cell-to-cell contact along the fiber length, ultimately biasing the manner in which cell-to-cell fusion occurs to elongate or 'grow' a myotube in a specific direction.

In this study, it should be noted that high levels of cell density (more than 90% confluent on the first day of the experiment) were required before differentiation would occur. Over the course of several days in culture, this results in cells growing on top of one another. As a result, cells that were not in direct contact with fibers may not have exhibited contact guidance. Thus, no attempt was made to quantify the degree of cell alignment because such quantification may not be reliable. However, cells in direct contact with non-printed (Fig. 2) or GF-soaked STEP fibers (Fig. 7) exhibited contact guidance by aligning along the fiber length.

To spatially control stem cell differentiation, polystyrene STEP fibers were coated with ECM molecules such as fibrin and printed with GFs that promoted musculoskeletal cell differentiation. This approach takes advantage of the phenomena that biological spatial patterning occurs, in part, by sequestration of GFs to the ECM and cell surfaces, and it seeks to recreate physiologically-relevant conditions by immobilizing spatially-defined patterns of GFs, in picogram to nanogram levels, to ECM surfaces [4,6,8–12]. To create such patterns, GFs that have heparin-binding domains, such as FGF-2, BMP-2 and heparin-binding EGF-like GF, are employed to immobilize them to appropriate ECM printing substrates via their native binding affinities [4,6,8–12]. Fibrin is one appropriate ECM material because of its inherent GF-binding capability as well as its physiological relevance as a provisional matrix during the wound healing process [38]. In addition, since serum contains a complex mixture of ECM proteins, it was utilized in this study (Fig. 3) to demonstrate that different ECM proteins can be used for immobilizing GFs as long as the ECM proteins possess inherent GF-binding capability [4]. BMP-2 and FGF-2 were employed here because previous studies have shown that these GFs can direct stem cells towards osteoblast and tenocyte differentiation, respectively [8,11,12,39,40]. In addition, we have previously shown that bioprinted GF patterns persist *in vivo* and can spatially promote or inhibit bone formation [7].

When C3H10T1/2 and C2C12 cells were seeded onto ECM-coated STEP fibers bioprinted with GFs, they differentiated appropriately on printed patterns (Figs 3,4,5 and 6). The differentiation markers used for myocytes, tenocytes and osteoblasts were Sarcomeric Myosin [41], Scleraxis [40,42–45] and Alkaline Phosphatase [46], respectively. Although several other differentiation markers such Eya [47], Six1 [48], Mohawk [49,50] and tenomodulin [51,52] are available for tenocytes, Scleraxis was utilized in this study as it is an early marker of tenocytes with highly specific expression in tendon progenitor cells and differentiating tendon cells [39,44,45]. In addition, Scleraxis expression is upregulated to coordinate injury response during tendon healing [53]. On serum-coated STEP fibers printed with FGF-2, C3H10T1/2 cells upregulated the tendon marker Scx in a dose-dependent manner, indicative of cells being driven towards a tenocyte fate (Fig. 3). On fibrin-coated STEP fibers printed with BMP-2, C2C12 cells upregulated the osteoblast marker ALP, indicative of cells being driven towards an osteoblast fate (Fig. 4). On fibrin-coated STEP fibers printed with FGF-2, C2C12 cells upregulated the tendon marker Scx in a dose-dependent manner, indicative of cells being driven towards a tenocyte fate (Fig. 5). Outside the printed region, myocytes aligned along the fiber length (Fig. 5).

To demonstrate that cell alignment and cell differentiation could be controlled simultaneously with oriented sub-micron fibers and multiple GFs, respectively, C2C12 cells were seeded on adjacent patterns of FGF-2 and BMP-2 printed onto fibrin-coated polystyrene STEP fibers. ALP and Scx expression increased on the BMP-2 and FGF-2 patterns, respectively, indicative of cells being driven towards osteoblast and tenocyte fates (Fig. 6). Outside of the printed region, aligned myocytes were observed (Fig. 6B). Interestingly, BMP-2 was shown to upregulate expression of the tendon marker Scx although at much lower levels than FGF-2 (Fig. 6B,D). This upregulation may be attributed to BMP-2 induced activation of the Smad signaling pathway, which has been previously shown to be involved in neotendon formation [54].The results shown here demonstrate that bioprinting of GFs onto aligned configurations of ECM-coated fibers can create a unique microenvironment that simultaneously controls cell differentiation and alignment, respectively.

5. Conclusion

This study focused on the characterization and systematic *in vitro* evaluation of a novel biomimetic, sub-micron fiber-based scaffold patterned with GFs to create biochemical and geometric cues that spatially direct a single stem cell population towards multiple cell fates, including tenocytes, myocytes or osteoblasts, while simultaneously controlling cell alignment within the same construct. The capability to spatially control stem cell orientation and differentiation towards multiple phenotypes simultaneously, allows cells grown *in vitro* to more closely mimic aspects of native tissue organization and structure. This capability offers a systematic approach to study the basic principles involved in tissue formation and function *in vitro* and may lead to bioinspired strategies for improved material design to treat musculoskeletal diseases and trauma.

Acknowledgements

We would like to thank Bur Chu and Larry Schultz for assistance with GF printing. We would also like to thank Dr. Haibing Teng for assistance with confocal microscopy. This work was supported by NIH grants RO1EB004343 and RO1EB007369 as well as funding from the Pennsylvania Infrastructure Technology Alliance (PITA). The MF20 monoclonal antibody developed by Donald A. Fischman was obtained from the Developmental Studies Hybridoma Bank developed under the auspices of the NICHD and maintained by The University of Iowa, Department of Biology, Iowa City, IA 52242. A. N and J. W are also thankful to Institute for Critical Technology and Applied Sciences (ICTAS) along with Nanoscale Characterization and Fabrication Laboratory (NCFL) at VT for SEM work.

Appendix. Supplementary information

Supplementary data related to this article can be found online at doi:10.1016/j.biomaterials.2011.07.025.

References

[1] Beniash E. Biominerals-hierarchical nanocomposites: the example of bone. Wiley Interdiscip Rev Nanomed Nanobiotechnol 2010;3:47–69.
[2] Fu RH, Wang YC, Liu SP, Huang CM, Kang YH, Tsai CH, et al. Differentiation of stem cells: strategies for modifying surface biomaterials. Cell Transplant 2010; 20:37–47.
[3] Nelson CM, Bissell MJ. Of extracellular matrix, scaffolds, and signaling: tissue architecture regulates development, homeostasis, and cancer. Annu Rev Cell Dev Biol 2006;22:287–309.
[4] Taipale J, Keski-Oja J. Growth factors in the extracellular matrix. FASEB J 1997; 11:51–9.
[5] Unsicker K, Krieglstein K. Cell signaling and growth factors in development. Germany: Wiley-VCH; 2006.
[6] Campbell PG, Miller ED, Fisher GW, Walker LM, Weiss LE. Engineered spatial patterns of fgf-2 immobilized on fibrin direct cell organization. Biomaterials 2005;26:6762–70.
[7] Cooper GM, Miller ED, Decesare GE, Usas A, Lensie EL, Bykowski MR, et al. Inkjet-based biopatterning of bone morphogenetic protein-2 to spatially control calvarial bone formation. Tissue Eng Part A 2010;16:1749–59.
[8] Ker ED, Chu B, Phillippi JA, Gharaibeh B, Huard J, Weiss LE, et al. Engineering spatial control of multiple differentiation fates within a stem cell population. Biomaterials 2011;32:3413–22.
[9] Miller ED, Fisher GW, Weiss LE, Walker LM, Campbell PG. Dose-dependent cell growth in response to concentration modulated patterns of fgf-2 printed on fibrin. Biomaterials 2006;27:2213–21.
[10] Miller ED, Li K, Kanade T, Weiss LE, Walker LM, Campbell PG. Spatially directed guidance of stem cell population migration by immobilized patterns of growth factors. Biomaterials 2011;32:2775–85.
[11] Miller ED, Phillippi JA, Fisher GW, Campbell PG, Walker LM, Weiss LE. Inkjet printing of growth factor concentration gradients and combinatorial arrays immobilized on biologically-relevant substrates. Comb Chem High Throughput Screen 2009;12:604–18.
[12] Phillippi JA, Miller E, Weiss L, Huard J, Waggoner A, Campbell P. Microenvironments engineered by inkjet bioprinting spatially direct adult stem cells toward muscle- and bone-like subpopulations. Stem Cells 2008;26:127–34.
[13] Hinds S, Bian W, Dennis RG, Bursac N. The role of extracellular matrix composition in structure and function of bioengineered skeletal muscle. Biomaterials 2011;32:3575–83.
[14] Shimizu K, Fujita H, Nagamori E. Alignment of skeletal muscle myoblasts and myotubes using linear micropatterned surfaces ground with abrasives. Biotechnol Bioeng 2009;103:631–8.
[15] Vye MV. The ultrastructure of striated muscle. Ann Clin Lab Sci 1976;6: 142–51.
[16] Gigante A, Cesari E, Busilacchi A, Manzotti S, Kyriakidou K, Greco F, et al. Collagen I membranes for tendon repair: effect of collagen fiber orientation on cell behavior. J Orthop Res 2009;27:826–32.
[17] Kerschnitzki M, Wagermaier W, Roschger P, Seto J, Shahar R, Duda GN, et al. The organization of the osteocyte network mirrors the extracellular matrix orientation in bone. J Struct Biol 2011;173:303–11.
[18] Ma J, He X, Jabbari E. Osteogenic differentiation of marrow stromal cells on random and aligned electrospun poly(l-lactide) nanofibers. Ann Biomed Eng 2011;39:14–25.
[19] Moffat KL, Sun WH, Pena PE, Chahine NO, Doty SB, Ateshian GA, et al. Characterization of the structure-function relationship at the ligament-to-bone interface. Proc Natl Acad Sci U S A 2008;105:7947–52.
[20] Moffat KL, Wang IN, Rodeo SA, Lu HH. Orthopedic interface tissue engineering for the biological fixation of soft tissue grafts. Clin Sports Med 2009;28:157–76.
[21] Erisken C, Kalyon DM, Wang H. Functionally graded electrospun polycaprolactone and beta-tricalcium phosphate nanocomposites for tissue engineering applications. Biomaterials 2008;29:4065–73.
[22] Munoz-Pinto DJ, McMahon RE, Kanzelberger MA, Jimenez-Vergara AC, Grunlan MA, Hahn MS. Inorganic-organic hybrid scaffolds for osteochondral regeneration. J Biomed Mater Res A 2010;94:112–21.
[23] Sahoo S, Ang LT, Goh JC, Toh SL. Growth factor delivery through electrospun nanofibers in scaffolds for tissue engineering applications. J Biomed Mater Res A 2010;93:1539–50.
[24] Sahoo S, Toh SL, Goh JC. A bfgf-releasing silk/plga-based biohybrid scaffold for ligament/tendon tissue engineering using mesenchymal progenitor cells. Biomaterials 2010;31:2990–8.
[25] Shi J, Wang L, Zhang F, Li H, Lei L, Liu L, et al. Incorporating protein gradient into electrospun nanofibers as scaffolds for tissue engineering. ACS Appl Mater Interfaces 2010;2:1025–30.
[26] Wang F, Li Z, Tamama K, Sen CK, Guan J. Fabrication and characterization of prosurvival growth factor releasing, anisotropic scaffolds for enhanced mesenchymal stem cell survival/growth and orientation. Biomacromolecules 2009;10:2609–18.
[27] Jose MV, Thomas V, Xu Y, Bellis S, Nyairo E, Dean D. Aligned bioactive multicomponent nanofibrous nanocomposite scaffolds for bone tissue engineering. Macromol Biosci 2010;10:433–44.
[28] Moffat KL, Kwei AS, Spalazzi JP, Doty SB, Levine WN, Lu HH. Novel nanofiber-based scaffold for rotator cuff repair and augmentation. Tissue Eng Part A 2009;15:115–26.
[29] Zhao Y, Zeng H, Nam J, Agarwal S. Fabrication of skeletal muscle constructs by topographic activation of cell alignment. Biotechnol Bioeng 2009;102: 624–31.
[30] Nain AS, Kowalewski T, Jacobson A, Sitti M, Amon C. Dry spinning based spinneret based tunable engineered parameters (step) technique for controlled and aligned deposition of polymeric nanofibers. Macromol Rapid Commun 2009;30:6.
[31] Nain AS, Phillippi JA, Sitti M, Mackrell J, Campbell PG, Amon C. Control of cell behavior by aligned micro/nanofibrous biomaterial scaffolds fabricated by spinneret-based tunable engineered parameters (step) technique. Small 2008; 4:1153–9.
[32] Miller E. Inkjet printing of solid-phase growth factor patterns to direct cell fate [Doctor of Philosophy]. Pittsburgh: Carnegie Mellon University; 2007.
[33] Engler AJ, Sen S, Sweeney HL, Discher DE. Matrix elasticity directs stem cell lineage specification. Cell 2006;126:677–89.
[34] Grosberg A, Kuo PL, Guo CL, Geisse NA, Bray MA, Adams WJ, et al. Self-organization of muscle cell structure and function. PLoS Comput Biol 2011;7: e1001088.
[35] Liu X, Chen J, Gilmore KJ, Higgins MJ, Liu Y, Wallace GG. Guidance of neurite outgrowth on aligned electrospun polypyrrole/poly(styrene-beta-isobutylene-beta-styrene) fiber platforms. J Biomed Mater Res A 2010;94: 1004–11.
[36] Tee SY, Fu J, Chen CS, Janmey PA. Cell shape and substrate rigidity both regulate cell stiffness. Biophys J 2011;100:L25–7.
[37] Zemel A, Rehfeldt F, Brown AE, Discher DE, Safran SA. Cell shape, spreading symmetry and the polarization of stress-fibers in cells. J Phys Condens Matter 2011;22:194110.
[38] Breen A, O'Brien T, Pandit A. Fibrin as a delivery system for therapeutic drugs and biomolecules. Tissue Eng Part B Rev 2009;15:201–14.
[39] Brent AE, Tabin CJ. Fgf acts directly on the somitic tendon progenitors through the ets transcription factors pea3 and erm to regulate scleraxis expression. Development 2004;131:3885–96.
[40] Cserjesi P, Brown D, Ligon KL, Lyons GE, Copeland NG, Gilbert DJ, et al. Scleraxis: a basic helix-loop-helix protein that prefigures skeletal formation during mouse embryogenesis. Development 1995;121:1099–110.
[41] Bader D, Masaki T, Fischman DA. Immunochemical analysis of myosin heavy chain during avian myogenesis in vivo and in vitro. J Cell Biol 1982;95: 763–70.
[42] Murchison ND, Price BA, Conner DA, Keene DR, Olson EN, Tabin CJ, et al. Regulation of tendon differentiation by scleraxis distinguishes force-transmitting tendons from muscle-anchoring tendons. Development 2007; 134:2697–708.
[43] Perez AV, Perrine M, Brainard N, Vogel KG. Scleraxis (scx) directs lacz expression in tendon of transgenic mice. Mech Dev 2003;120:1153–63.
[44] Pryce BA, Watson SS, Murchison ND, Staverosky JA, Dunker N, Schweitzer R. Recruitment and maintenance of tendon progenitors by tgf {beta} signaling are essential for tendon formation. Development 2009; 136:1351–61.
[45] Schweitzer R, Chyung JH, Murtaugh LC, Brent AE, Rosen V, Olson EN, et al. Analysis of the tendon cell fate using scleraxis, a specific marker for tendons and ligaments. Development 2001;128:3855–66.
[46] Henrichsen E. Alkaline phosphatase in osteoblasts and fibroblasts cultivated in vitro. Exp Cell Res 1956;11:115–27.
[47] Xu PX, Cheng J, Epstein JA, Maas RL. Mouse eya genes are expressed during limb tendon development and encode a transcriptional activation function. Proc Natl Acad Sci U S A 1997;94:11974–9.
[48] Boucher CA, Carey N, Edwards YH, Siciliano MJ, Johnson KJ. Cloning of the human six1 gene and its assignment to chromosome 14. Genomics 1996;33: 140–2.

[49] Anderson DM, Arredondo J, Hahn K, Valente G, Martin JF, Wilson-Rawls J, et al. Mohawk is a novel homeobox gene expressed in the developing mouse embryo. Dev Dyn 2006;235:792–801.
[50] Liu W, Watson SS, Lan Y, Keene DR, Ovitt CE, Liu H, et al. The atypical homeodomain transcription factor mohawk controls tendon morphogenesis. Mol Cell Biol 2010;30:4797–807.
[51] Shukunami C, Takimoto A, Oro M, Hiraki Y. Scleraxis positively regulates the expression of tenomodulin, a differentiation marker of tenocytes. Dev Biol 2006;298:234–47.
[52] Docheva D, Hunziker EB, Fassler R, Brandau O. Tenomodulin is necessary for tenocyte proliferation and tendon maturation. Mol Cell Biol 2005;25:699–705.
[53] Scott A, Sampaio A, Abraham T, Duronio C, Underhill TM. Scleraxis expression is coordinately regulated in a murine model of patellar tendon injury. J Orthop Res 2011;29:289–96.
[54] Hoffmann A, Pelled G, Turgeman G, Eberle P, Zilberman Y, Shinar H, et al. Neotendon formation induced by manipulation of the smad8 signalling pathway in mesenchymal stem cells. J Clin Invest 2006;116:940–52.